First-principles study of titanium oxides

Chinmong Leung
Department of Physics, State University of New York at Stony Brook, Stony Brook, New York 11794-3800

M. Weinert
Department of Physics, Brookhaven National Laboratory, Upton, New York 11973–5000

Philip B. Allen
Department of Physics, State University of New York at Stony Brook, Stony Brook, New York 11794-3800

Renata M. Wentzcovitch
Minnesota Supercomputer Institute and Department of Chemical Engineering and Materials Science, University of Minnesota, Minneapolis, Minnesota 55455

(Received 9 May 1996)

Titanium forms a wide range of stoichiometric oxides. The low-temperature monoclinic phase of titanium monoxide Ti_5O_5 has an ordered array of vacancies in an otherwise simple NaCl structure. Using the variable cell shape method and the local-density approximation, all 12 parameters of the crystal structure are relaxed. Comparisons with other possible structures and other transition-metal monoxides suggest that there is a competition between kinetic- and Madelung-energy contributions and that this low symmetry structure is stabilized in part by the overlap of occupied Ti-ion orbitals via the vacant oxygen site. Resistivities of the low-temperature Ti_5O_5 phase fitted using the Bloch-Grüneisen formula imply that the monoxide is a borderline quasiparticle gas. [S0163-1829(96)04835-7]

I. INTRODUCTION

Many oxides, carbides, and nitrides of the group-IVa and -Va metals crystallize in the simple NaCl (rocksalt) -type structure at compositions near one to one.[1] These compounds generally exhibit a wide composition range depending on temperatures and pressures.[2] In an otherwise perfect NaCl structure, the compound may crystallize with varying amounts of titanium and oxygen vacancies, resulting in a nonstoichiometric chemical formula TiO_x with x ranging from 0.7 to 1.25. At a composition $TiO_{0.7}$, the titanium sublattice is almost completely occupied, but about one-third of the oxygen sites are vacant, while for $TiO_{1.25}$, the oxygen lattice is almost filled and about one-quarter of the titanium sites are vacant. For $x=1$ and temperatures above 990 °C, there are $\sim$15% random vacant sites on both the titanium and oxygen sublattices; annealing at 990 °C causes the vacancies to order[3] on the underlying NaCl lattice. This ordered phase has monoclinic symmetry, with a chemical formula corresponding to Ti_5O_5 in the primitive cell. In the cubic phase, the resistivity of cubic TiO_x is essentially independent of both temperature and composition. However, when the vacancies order, the electrical resistivity is drastically reduced. The resistivity temperature coefficient $(d\rho/dT)$ becomes positive showing normal metallic character. The superconducting T_c is around 0.6 K and not very sensitive to vacancy ordering, but increases to 2.3 K when vacancies are eliminated under pressure. For TiO_x, there is no indication of spontaneous magnetic ordering at low temperature. A common feature of these compounds is that the vacancy concentration is relatively independent of preparation temperature, implying that vacancies are an important contribution to the internal energy of the crystal.

In this paper we use first-principles electronic-structure calculations to address a number of questions. What is the influence of vacancies on stoichiometric TiO? Why does this oxide crystallize in such a low symmetry form, while other transition-metal monoxides crystallize in the simple NaCl structure? Nb_3O_3 also has ordered vacancies, but in a simpler arrangement; why does Ti_5O_5 avoid such simplicity? Previously, both non-self-consistent[4,5] and self-consistent[6] calculations have been used to discuss the band structure of rocksalt TiO. Here we ask whether it is possible to trace the important features of Ti_5O_5 back to simple features in the rocksalt structure.

In Sec. II we introduce the structures studied and the method of calculation. The heats of formation of titanium oxides and their relative structural stability are discussed in Sec. III. In Sec. IV we discuss the electronic structure and try to address the stability of the vacancy ordered structure. The resistivity is analyzed in Sec. V and we summarize our results in Sec. VI.

II. CRYSTAL STRUCTURES AND CALCULATIONS

When carefully annealed, TiO undergoes a first-order phase transition at 990 °C from the NaCl structure to a monoclinic structure with space group $A2/m$.[3] The high-temperature phase has $\sim$14.6% randomly arranged vacancies, while in the low-temperature phase the vacancies become ordered. Since there is approximately one formula unit missing in every six units, we denote this stoichiometric compound Ti_5O_5.

For comparison, we also consider two other structures. In

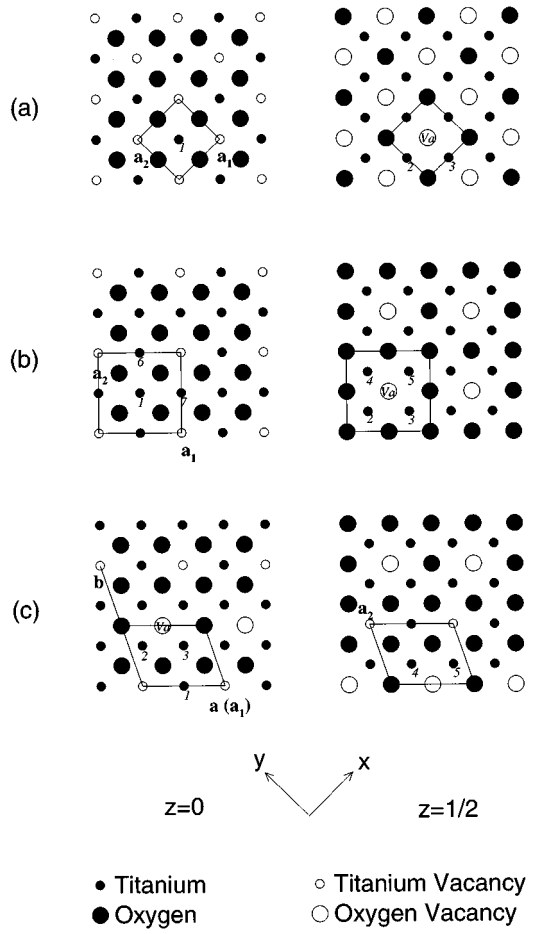

FIG. 1. Crystalline structures of (a) Ti_3O_3, (b) Ti_7O_7, and (c) Ti_5O_5. Solid lines are the boundaries of the primitive unit cells projected onto the x-y plane. The left- (right-) hand side figures correspond to the $z=0$ ($z=\frac{1}{2}a_3$) plane. Numbers on the figures label Ti ions in the corresponding unit cells. Note that $\mathbf{a}_2$ of Ti_5O_5 has a nonvanishing z component.

Fig. 1 all three lattices consist of two nonequivalent layers of ions with the second layer at $z=\mathbf{a}_3/2$ ($\mathbf{a}_3$ is the common third primitive lattice vector). When all lattice sites are occupied by the corresponding type of ions, all three lattices are simply the rocksalt structure. In structure (a), denoted Ti_3O_3, 25% of the lattice sites are vacant and the primitive unit cell has three TiO units per cell. This crystal structure shares many similarities with Ti_5O_5 and is the structure actually observed in niobium oxide. The second structure (b) is designed to have the local environment of the anion vacancy as similar as possible to that in the monoclinic phase and has a vacancy concentration of 12.5%; there is no evidence that this structure actually exists, but it is useful in understanding the actual structure. Finally, (c) is the actual ordered vacancy structure. All three lattices have an underlying rocksalt matrix of metal and oxygen ions and have an anion (cation) vacancy surrounded by six octahedrally coordinated cations (anions) and 12 next-nearest-neighbor anions (cations). The differences among them occurs for third and higher neighbors, where the vacancy concentration plays an important role. In structure (a) the lattice constant is the only free parameter. In Ti_5O_5, the presence of the vacancies dramatically reduces the symmetry. There are 12 free parameters required to completely specify the structure: three lattice constants a,b,c and an angle γ for the cell shape, and eight internal degrees of freedom.

TABLE I. Theoretical and experimental structural parameters of Ti_5O_5. The definitions of the parameters together with their experimental values are given in Ref. 2.

Parameter	Experiment	Calculation
a	5.855 Å	5.730 Å
b	9.340 Å	9.278 Å
c	4.142 Å	4.136 Å
γ	107°32′	107°
(x_1,y_1)	(0.170, 0.340)	(0.172, 0.340)
(x_2,y_2)	(0.669, 0.342)	(0.668, 0.355)
(x_3,y_3)	(0.343, 0.175)	(0.344, 0.173)
(x_4,y_4)	(0.833, 0.179)	(0.832, 0.174)

In order to find the local-density approximation (LDA) ground state structure, we perform a full relaxation of these structures, using a damped version of the variable cell shape molecular-dynamics method.[7] In this method, fully self-consistent solutions of the one-electron equation[8] are found at each time step. To relax the Ti_5O_5 structure requires about 20 steps. The pseudopotentials are generated using the Troullier-Martins[9] scheme and the Ceperly-Alder[10] exchange-correlation potential as parametrized by Perdew and Zunger.[11] The potentials are transformed into separable form using the Kleinman-Bylander procedure[12] and the p and s components are chosen as the local potential for oxygen and titanium, respectively.

III. STRUCTURAL STABILITY AND HEATS OF FORMATION

The structural parameters for Ti_5O_5 given in Table I all agree with experiment within 2%. Plots of the total energy versus volume for various phases are shown in Fig. 2. The

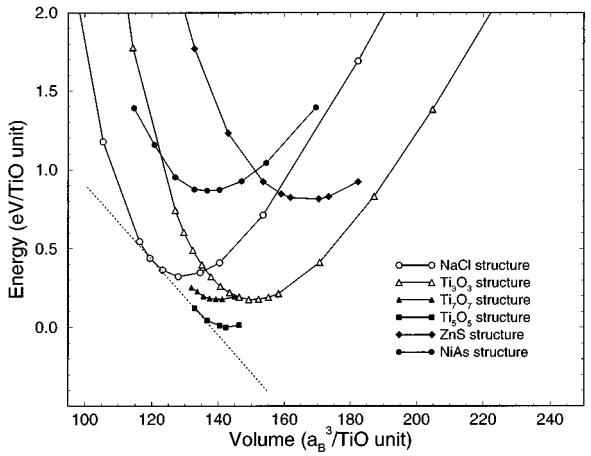

FIG. 2. Relative total energies per TiO unit versus volume for various structures. The dotted line is the common tangent between the Ti_5O_5 and rocksalt curves.

TABLE II. Heats of formation of titanium oxides in eV/atom. Experimental data are from Ref. 31.

Oxide	Experiment	Calculation
TiO	−2.68	−3.36
Ti_2O_3	−3.14	−3.66
TiO_2	−3.26	−3.68

low-temperature form Ti_5O_5 is found to be the stablest and all three defective phases are more stable than the rocksalt structure. As predicted by crystal field theory, the most stable phases contain Ti ions in octahedral rather than tetrahedral sites (ZnS structure). Consistent with empirical statements, we also find that the NiAs structure, which has extensive face-sharing octahedrons, is not favored by this oxide.

The results shown suggest it should be possible to induce a phase transformation to the defect-free rocksalt phase by applying pressure. The slope of the common tangent in Fig. 2 indicates a transition pressure of ~25 GPa from Ti_5O_5 to rocksalt TiO. Experimentally, such a transformation is found with a transition pressure[13] of 7.7 GPa for a sample containing 14.4% random vacancies. The rather large discrepancy between the calculated and experimental pressures may in part be due to the random ordering of the vacancies in the sample, which destroys the local environment of the empty oxygen site; the energy of a system with random vacancies should be higher in internal energy than that of the ordered Ti_5O_5 phase, implying a lower transition pressure. Thus the predicted transition pressure of 25 GPa should be a loose upper bound to the experimental value for random vacancies.

Titanium is unusual in that it forms many crystalline compounds with oxygen. The sesquioxide Ti_2O_3 has the corundum structure and has a number of interesting properties driven by temperature: It is semiconducting with a small gap 0.2 eV below 390 K,[14] but becomes metallic at higher temperature. Accompanying this metal-nonmetal transition, there is an anomalous change in the lattice constants and internal coordinates but no known change in symmetry.[15] The dioxide TiO_2 is a polymorphic insulator, with rutile being the most common structural phase. Other observed phases include anatase, brookite, and a recently discovered $TiO_2(B)$.[16] All these phases are similar in that the Ti ions are octahedrally coordinated by oxygens and that metal-metal bonds are formed to varying degree. Using the same methods as described in Sec. II, we obtain the total energies of these stable titanium oxides, together with the energy for crystalline titanium and molecular[17] O_2. Heat of formations are then calculated by

$$\Delta H(Ti_{1-x}O_x) = E_{tot}(Ti_{1-x}O_x) - (1-x)E_{tot}(Ti) - x\,\tfrac{1}{2}E_{tot}(O_2), \quad (1)$$

where x is the oxygen concentration of the binary compounds and $x=0.5$, 0.6, and 2/3, corresponding to TiO, Ti_2O_3, and TiO_2 (rutile), respectively. As shown in Table II and Fig. 3, the calculations show the correct trend compared to experiment. TiO_2 (rutile) is found to be the most stable, but the heats of the monoxide and sesquioxide are below the line joining the heat of Ti and TiO_2. Therefore, in agreement with experiment, all phases are predicted to exist and it should be possible to produce these oxides by reducing titanium dioxide with titanium metal; the Ti_5O_5 and Ti_2O_3 samples used for the x-ray-diffraction structure determination[18] were in fact prepared in this way.

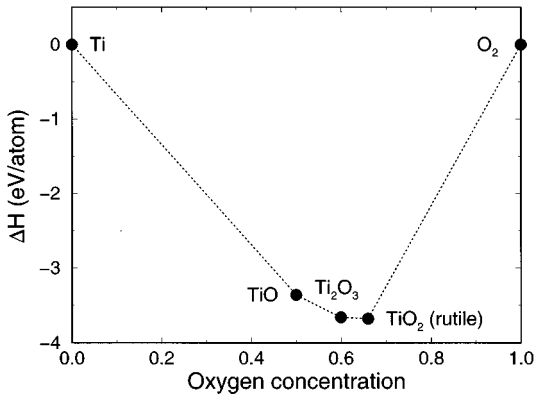

FIG. 3. Calculated heats of formation (eV/atom) of three stable titanium oxides.

IV. ELECTRONIC STRUCTURE

The energy bands and density of states (DOS) for the ideal rocksalt structure and the different vacancy structures are shown in Figs. 4 and 5, respectively. The bands for the rocksalt structure in Fig. 4 are given in the same (super)cell as for Ti_5O_5 in order to show the band foldings and interactions (anticrossings) resulting from the existence of the

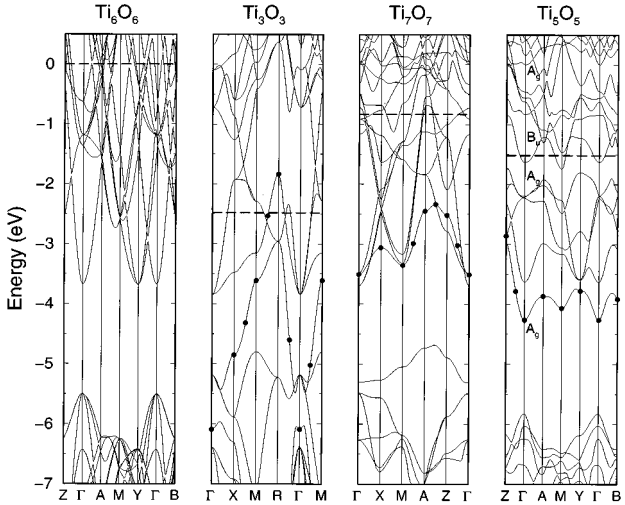

FIG. 4. Energy bands along the symmetry lines for rocksalt (Ti_6O_6) and the crystal structures given in Fig. 1. The bands marked with dots have increased electron density at the vacant oxygen site. Fermi levels are marked by horizontal dashed lines. The notation for the symmetry points for the Ti_3O_3 and Ti_7O_7 bands are standard (Ref. 30). The notations for Ti_6O_6 (folded NaCl) and Ti_5O_5 are $\Gamma=(0,0,0)$, $A=(\frac{1}{2},0,0)$, $M=(\frac{1}{2},\frac{1}{2},0)$, $Y=(0,\frac{1}{2},0)$, $Z=(0,\frac{1}{4},\frac{1}{2})$, and $B=(\frac{1}{2},\frac{1}{4},0)$. The first four points have the full point-group symmetry of the crystal (C_{2h}) and the small group of the last two points is C_2.

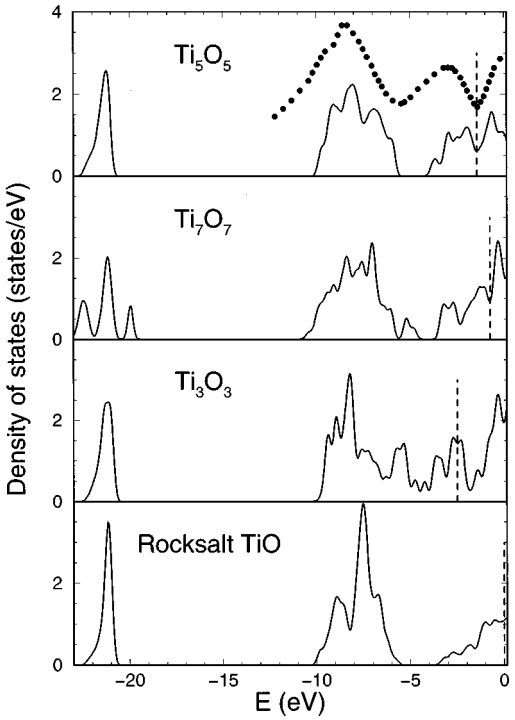

FIG. 5. Density of states (per TiO unit) corresponding to the bands in Fig. 4. Full circles are x-ray K emission and L_{III} absorption spectra from Ref. 19.

vacancies. Note that because of the difference in vacancy concentration, the band fillings will be different; in a simple rigid band model, the Fermi levels would be different for each structure. To make comparisons among the different structures, we have aligned the position of the O 2s states rather than the Fermi levels. The justification for this choice is that the ''bulklike'' oxygen atoms (those ''far'' away from the Ti and O vacancies) should have similar electronic properties and densities; if their environments were identically the same, the core levels on these atoms would provide a common reference level. Although the O 2s states are not strictly core states, they are far enough below the Fermi level and have small enough spatial extent to provide a reasonable approximation. That this choice is reasonable—and significantly better than aligning Fermi levels—can be seen by comparing the DOS in Fig. 5: Not only are the O 2s states aligned, but the O ''2p'' (between approximately -10 and -6 eV) and Ti ''3d'' bands are aligned, while the Fermi level shifts are several eV.

In Fig. 5 the x-ray emission and absorption data[19] are compared with the DOS of the ordered Ti_5O_5 structure. The overall agreement is reasonable, including the minimum at the Fermi level. The presence of vacancies modifies the bands and the density of states throughout the O 2p and Ti 3d regions, with the Ti_3O_3 structure showing the largest changes in the DOS.

The eigenstates with significant weight in the empty oxygen site are marked with dots in Fig. 4. These states have eigenvalues consistently lower compared to others in the d manifold and for Ti_3O_3 are responsible for the density of states between the O 2p and Ti 3d bands. Indeed these vacancy-derived states constitute the lowest d band for the

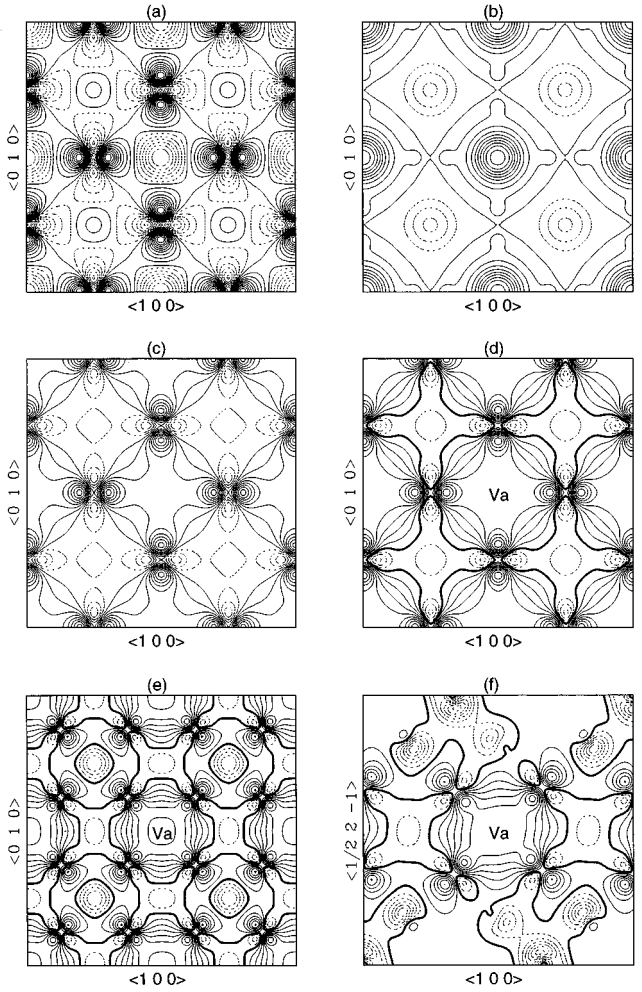

FIG. 6. Contour plots of the Bloch (pseudo)functions for TiO in the ideal Ti_4O_4 structure at Γ for (a) the 35th band (ψ_{35}), (b) the 4th band (ψ_4), and (c) $1/\sqrt{2}(\psi_{35}+\psi_4)$. The zone center vacancy-derived states for (d) Ti_3O_3, (e) Ti_7O_7, and (f) Ti_5O_5 in the planes given in Fig. 1 are also given. Successive contours are separated by $0.5\Omega^{-1}$, where Ω is the volume over which the Bloch functions are normalized; the thick contours correspond to zero and negative contours are dashed. The anion (oxygen) vacancies are marked by ''Va.''

Ti_5O_5 structure throughout the entire Brillouin zone (BZ). As discussed below, these states can be considered as the bonding levels of a bonding-antibonding pair. In a simple single-particle picture, the occupation of the bonding levels, but not of the antibonding ones, implies a gain of crystal stability with respect to rocksalt TiO. While this is a plausible argument for the stability of Ti_5O_5, a more complete description must include the ''double counting'' (Coulomb) terms and the changes of all the states. In addition, the dips in the DOS at the Fermi level seen in Fig. 5 for the vacancy structures are also consistent with increased stability in such a simple model.

A better understanding of the formation of the vacancy states is provided by real-space plots of the vacancy state Bloch functions. The zone center vacancy states on the x-y plane centered at the empty oxygen site are shown in Figs. 6(d)–6(f) for Ti_3O_3, Ti_7O_7, and Ti_5O_5, respectively. A common feature in all these plots is that the neighboring Ti

orbitals surrounding the empty oxygen site overlap through the vacancy. Integration of the self-consistent charge density inside a sphere of nominal O^{--} (Ti^{++}), with a radius of $2.49a_B$ ($1.78a_B$), at the empty oxygen (titanium) sites give 1.86, 1.74, and 2.14 (0.20, 0.14, and 0.14) electrons for Ti_3O_3, Ti_7O_7, and Ti_5O_5, respectively. This rather large amount of charge at the oxygen vacancy site includes the contributions from all occupied states, but is dominated by the vacancy states. Note that the oxygen vacancy site is effectively a doubly charged anion, just as if an oxygen atom were there. Although this observation might be considered as evidence for the ionic character of TiO, there is also significant covalent character. Using Pauling's[20] ionic scale and calculating the amount of charge rearrangement relative to the superposition of neutral spherical atoms, we estimate $\sim$40% covalent character in the Ti-O bond; similarly, there is a considerable degree of covalency between metal ions.

It is instructive to use a tight-binding picture to discuss the vacancy-induced states. The zone center vacancy state for Ti_3O_3 shown in Fig. 6(d) is clearly made up of d-like orbitals at the Ti sites and s-like orbitals at the O vacancy site. For all the cases considered in this paper the vacancy orbital centered on the oxygen vacancy can be described by the combination of atomic orbitals

$$\phi_{\rm vac}(\mathbf{r}) = a_1\phi^{(1)}_{3x^2-r^2}(\mathbf{r}) + a_2\phi^{(2)}_{3y^2-r^2}(\mathbf{r}) + a_3\phi^{(3)}_{3z^2-r^2}(\mathbf{r}) + b\,\phi_s(\mathbf{r}). \quad (2)$$

The d orbitals on the neighboring six Ti sites all point towards the oxygen vacancy site; the six Ti orbitals are reduced to three nonequivalent ones by inversion symmetry. The superscripts refer to the Ti atoms along the three axes. The last term ϕ_s is completely symmetric in x, y, and z and has the symmetry of an O s function. This linear combination also has been called a ''vacuum'' orbital.[21] For Ti_3O_3, all the a_i coefficients are equal because the three Ti ions are related by various symmetry operations, while for Ti_7O_7, $a_2 = a_3$ because of the C_{4z} symmetry operation. The lower symmetry of Ti_5O_5 does not require any particular relationships among the a_i coefficients.

While the plots of the vacancy state suggest that this combination is correct, a further justification of this combination starting from Ti_3O_3 can be constructed that makes connection to the ideal rocksalt bands. We start with the Ti_4O_4 rocksalt supercell and use this complete set of wave functions as a basis to describe the vacancy states. To go from Ti_4O_4 to Ti_3O_3, we introduce a vacancy potential; this perturbation has the same translation symmetry as the supercell so only states at the same k will mix. The states at the zone center of Ti_4O_4 are simply the states at Γ and the three X points of the primitive rocksalt structure because of the folding of the BZ. In the expansion, only states of Ti_4O_4 belonging to the Γ_1 irreducible representation of the group O_h are included because the vacancy state belongs to this representation. Not all the X (Γ) states of the primitive rocksalt TiO give rise to Γ_1 states at the zone center of Ti_4O_4. States belonging to the X_1 irreducible representation fold back to states with Γ_1 or Γ_{12} symmetry. From the TiO band structure as calculated by Mattheiss[5] and by Neckel *et al.*[1,6] (and confirmed by us), the lowest X_1 state at 1.6 Ry below the Fermi level comes mainly from oxygen $2s$ orbitals (corresponding to ϕ_s) and is shown in Fig. 6(a). The next higher X_1 state is 0.2 Ry above the Fermi level and originates from $d_{x^2-y^2}$ and $d_{3z^2-r^2}$ Ti orbitals. The symmetric combination of the X_1 ($d_{3z^2+r^2}$) states arising from the three different X points of the primitive cell is the Γ_1 state shown in Fig. 6(b). (The $d_{x^2-y^2}$ components fold into states with Γ_{12} symmetry.) For simplicity, we expand the vacancy state of Ti_3O_3 into only these two Γ_1 Ti_4O_4 states with equal weight and plot the resulting $\phi_{\rm vac}$ in Fig. 6(c). The great similarity between this two-state expansion picture and the actual self-consistent state of Fig. 6(d) suggests that the vacancy orbital expression is correctly constructed. Further support is provided by the calculated high degree of overlap of 0.91 between the self-consistent vacancy state and this simple linear combination.[22]

The Γ_1 vacancy state is the bonding combination of the low-lying oxygen s (Γ_1) state coupled with the high-lying Γ_1 Ti $3d$ states, resulting in a very dispersive vacancy-derived band. At the zone center, the antibonding vacancy state is 8.5 eV above the corresponding bonding vacancy state. States of other symmetry do not have the same large overlap with the vacancy potential and are not expected to have the same large interactions. Although smaller, there is, however, still a noticeable dispersion for the $\Gamma_{25'}$ states, which can be thought of as Ti d orbital overlapping along the edge of the empty oxygen site.

The analysis for Ti_5O_5 proceeds along the same lines. This crystal structure has additional complications due to the lower symmetry $A2/m$ (C_{2h}). Of the three X-point rocksalt states mentioned above, only two are folded back to zone center A_g states. (We switch notation for Ti_5O_5 to emphasize the differences.) The other X state folds to the interior point Δ. The third zone face state required to construct $\phi_{\rm vac}(\mathbf{r})$ is provided by two s states of primitive rocksalt TiO at $k=(\frac{1}{3},\frac{1}{3},-\frac{1}{3})$ and $k=(-\frac{1}{3},-\frac{1}{3},\frac{1}{3})$, which together fold back to $A_g + B_u$ at the zone center. The corresponding eigenvalues are almost degenerate with the X-point eigenvalues. Starting from these three A_g states, one can proceed with the same analysis as for Ti_3O_3. Because of the low symmetry of the crystal, there are more A_g states than Γ_1 states in Ti_4O_4. For example, two of the A or Ξ interior points of primitive TiO also fold back into zone center states ($A_g + B_u$). The vacancy-derived band is consequently less dispersive; in fact, the band energy of Ti_5O_5 is higher than that of Ti_3O_3, as in the self-consistent calculation.

There are other differences between the two structures. The four Ti ions of Ti_5O_5 surrounding the empty oxygen site on the x-y plane have an oxygen located on the other side. These oxygen atomic orbitals form antibonding states with the Ti atomic orbitals as shown in Fig. 6(f). The effect is to push more electron density towards the empty oxygen site. The valence electrons spreading into the empty sites have two consequences: (i) a lowering of the electron kinetic energy and (ii) recovery of part of Madelung energy lost because of the presence of the vacancies. Thus, although Ti_3O_3 is more stable than rocksalt TiO, it is still less bound than Ti_5O_5, which gains more in the electrostatic (double counting) part of the total energy. This argument is qualitatively shown in Fig. 7, where the Ewald and kinetic-energy

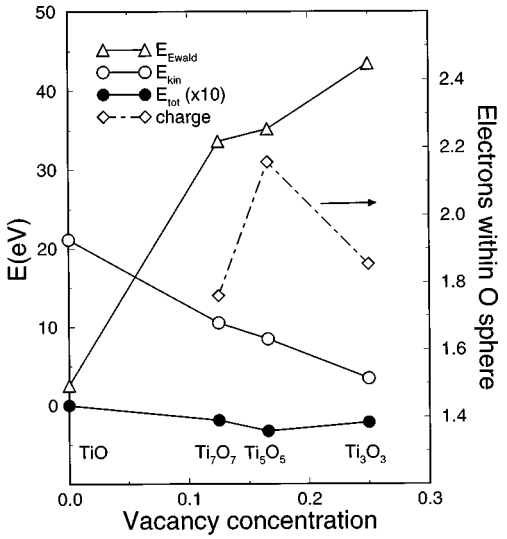

FIG. 7. Ewald, kinetic, and total energies (eV/TiO) for titanium monoxides versus vacancy concentration. The Ewald and kinetic energies have been rigidly shifted and the total energies have been multipled by a factor of 10 for clarity. Also shown is the number of electrons enclosed in a sphere with nominal ionic radius 1.32 Å centered at the oxygen vacancy site.

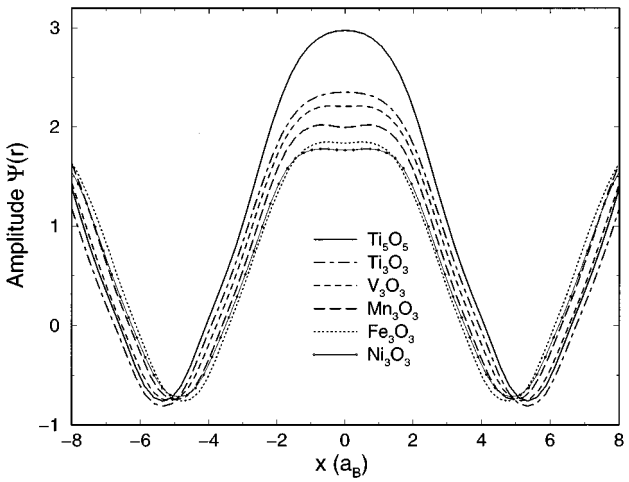

FIG. 8. Amplitude of the Bloch (pseudo)functions corresponding to Fig. 6 for Ti_5O_5 and selected 3*d* transition-metal oxides in the Ti_3O_3 structure in the $\mathbf{a}_1+\mathbf{a}_2$ direction passing through an empty oxygen site. All structures are fully relaxed. $x=0$ of the plot corresponds to the empty oxygen site and the two minimum points correspond to occupied oxygen sites.

contributions are shown to be monotonic increasing and decreasing functions, respectively, of the vacancy concentration. However, the amount of charge enclosed in a sphere centered at the empty oxygen site has a maximum at $\frac{1}{6}$, matching the concentration where the total energy of the monoxide is lowest.

These arguments are general and should be applicable to all transition-metal oxides in this structural form. However, the monoxides of the late 3*d* transition metals form mainly in the rocksalt structure. To investigate this question, we have examined V, Mn, Fe, and Ni oxides in the Nb_3O_3 (Ti_3O_3) structure. The same set of vacancy derived states are observed, as expected from the arguments given above. The corresponding zone center bonding-antibonding splitting of the vacancy states diminishes as one moves along the row; for the end member Ni_3O_3, the splitting is 7.9 eV compared to 8.5 eV for Ti_3O_3. The Fermi level is still below the zone center antibonding vacancy states, indicating that there is still some kinetic energy gained by forming the vacancy. However, the loss in Madelung energy is greater and the self-consistent calculation shows that rocksalt NiO is 0.1 eV more stable.

As a measure of the distribution of charge, we plot the Bloch function of these vacancy states across the empty oxygen site in Fig. 8. Although the optimum (relaxed) oxide cell volumes become smaller across the row, the magnitude of the wave functions also are decreasing in this empty site region. The more contracted metal ion orbitals are not able to overlap effectively and there is less metal-metal bonding in the late transition-metal oxides. For these oxides, the reduction of kinetic energy obtained by expanding into the vacancy site is not enough to compensate for the attendant loss of Madelung energy. Therefore, the vacancy structure is only suitable for large *d* orbital (early) transition-metal oxides. This figure also shows that the Ti_5O_5 structure is able to take better advantage of bonding across the vacancy than the Ti_3O_3 because of the Ti-O antibonding effect described above even though the interatomic distances are very close.

The model we have presented for the bonding of the TiO with vacancies is not the only possible one. Another approach to explain the formation of trapped electrons uses the hybrid orbital method.[23] According to this model, linear combinations of the Ti *d* orbitals at the corner of the octahedron form three-center hybrid bonding orbitals directed toward each of the eight equilateral triangles. These bonding orbitals are responsible for the formation of the energy band below the Fermi level. A consequence is that charge will pile up at the center of these triangles rather than at the center of the vacancy sites as predicted by our model. Our first-principles (deformation) densities show that the densities on these triangles are significantly smaller than the values near the center of the oxygen vacancy site. Hence, in our opinion it is more natural to describe the bonding in terms of the vacancy orbitals as given above rather than hybrid orbitals.

V. TRANSPORT PROPERTIES

The calculated band structure of Ti_5O_5 (cf. Fig. 4) has two energy bands crossing the Fermi level. Experimentally, TiO is metallic at room temperature and the electrical resistivity decreases with temperature. The positive metallic temperature coefficient is an indication that Ti_5O_5 may be a conventional electrical conductor. NbO also has an ordered vacancy structure (Ti_3O_3) and has been shown to be a conventional conductor.[24] Among the 3*d* transition-metal monoxides, only the titanium and vanadium oxides are conducting. VO also has a broad range of composition, but the resistivities become larger as the temperature is lowered. This behavior suggests that the conduction electron states in VO are not simple band states. Similar to the structural analysis above, there seems to be a boundary between Ti and V beyond which correlation effects become important. In

this section we study whether Ti_5O_5 fits into the category of conventional metals.

For conventional metals,[25] electric current is carried by a nonequilibrium distribution of quasiparticles. These excited electrons interact with sample impurities, phonons, and other electrons. In ordinary clean metals, the electron-phonon interaction dominates at room temperature and the electron-impurity interaction dominates at low temperatures. Coulomb interactions contribute only a small amount due to the limited phase space available. The nonequilibrium distribution $F(k)$ is determined by the Boltzmann equation and, in turn, determines the current

$$J=\sigma E=-\frac{e}{\Omega}\sum_k v_k F(k), \tag{3}$$

where k denotes both the wave vector and the band index of the quasiparticle states and Ω is the sample volume. Using an approximate variational solution to the Boltzmann equation, the conductivity tensor can be expressed as

$$\sigma_{\alpha\beta}=(n/m)_{\alpha\beta}e^2\tau. \tag{4}$$

The quantity (n/m) is the inverse effective mass tensor summed over all occupied states and is related to the Drude plasma frequency tensor by

$$\Omega^2_{P\alpha\beta}=4\pi(n/m)_{\alpha\beta}e^2=\frac{4\pi e^2}{\Omega}\sum_k v_{k\alpha}v_{k\beta}\delta(\epsilon_k-\epsilon_F). \tag{5}$$

One may calculate the group velocities of the electrons in these quasiparticle states from band theory and then construct the (n/m) tensor accordingly. Since density-functional theory was designed to produce energy spectra suitable for ground state properties, using the LDA bands to calculate the quasiparticle group velocities is an approximation. However, the validity of this approximation has been tested in the past for elemental metals and compounds[26–28] and the LDA values of the Drude plasma frequency appear to be reliable for nonmagnetic elements.

In these equations, the inverse scattering rate τ is a variational parameter in the Boltzmann equation. Its optimum value in the case of electron-phonon interaction can be expressed in closed form. If a Debye model is made for the phonon spectrum and matrix elements are simplified, this closed form expression is the Bloch-Grüneisen formula

$$\frac{4\pi\hbar}{\tau\lambda_{tr}k_B\Theta_D}=(4\pi)^2\left(\frac{2T}{\Theta_D}\right)^5\int_0^{\Theta_D/2T}dx\,\frac{x^5}{\sinh^2 x}, \tag{6}$$

where λ_{tr} is the electron-phonon coupling constant and is closely related to the superconducting transition temperature T_c through the McMillan equation. The Debye temperature is obtained from phonon dispersions measured by neutron scattering. The last parameter ρ_0 is the resistivity due to impurities, which is sample dependent. With the two parameters Θ_D and ρ_0 and the corresponding T_c of a material, this theory describes the resistivities of many elemental metals and a number of compounds very well.

The linear tetrahedron interpolation method is used to calculate the plasma frequencies. Because of the low symmetry (four operations) of the crystal, 744 k points in the irreducible Brillouin zone are needed to get converged results. The second rank plasma frequency tensor has six nonzero values. To make a comparison with experiment on polycrystalline samples containing many randomly oriented single crystals, the three eigenvalues are averaged to $\Omega_p=2.67$ eV. Using the Bloch-Grüneisen formula fitted to the experimental resistivity data with $\rho_0=58$ $\mu\Omega$ cm and $\Theta_D=500$ K, the electron-phonon coupling constant λ_{tr} is 1.2.

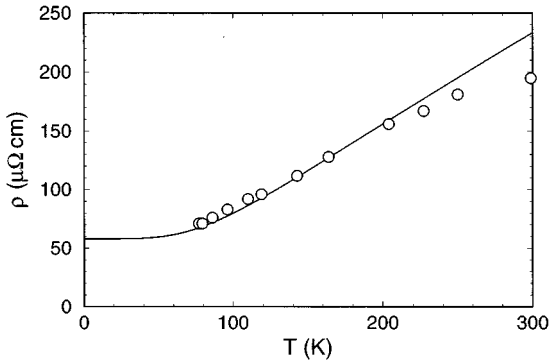

FIG. 9. Temperature dependence of resistivities of Ti_5O_5. Open circles are experimental data and the solid curve is a fit using the Bloch-Grüneisen formula.

The results of this fit and the experimental results are shown in Fig. 9. Although there is reasonable overall agreement with the data, there are some discrepancies. The value of λ_{tr} is larger than expected from the electron-phonon mass enhancement λ obtained for $T_c = 1.0$ K from the McMillan formula. Also with this fitted coupling constant, the calculated lifetime broadening at 300 K, $N(\epsilon_f)\hbar/\tau=0.4$, barely fulfills the first requirement for the validity of the Boltzmann equation, i.e., $N(\epsilon_f)\hbar/\tau\ll 1$. The calculated mean free path already reaches the critical value $l=10$ Å at 220 K. Similarly, the requirement $l\gg a$ is barely satisfied. Above this temperature, it appears that the experimental data rise less rapidly than predicted from the Boltzmann equation. This ''resistivity saturation''[29] is a common phenomenon and is qualitatively understood as due to the short quasiparticle lifetime that invalidates the Fermi liquid assumptions upon which the analysis is based. The fitted curve and the data match reasonably well below 220 K.

Based on the above analysis, Ti_5O_5 may still belong to the class of conventional metals, but its behavior is starting to deviate from a quasiparticle gas of conventional metals. VO, the next monoxide in the 3d row, shows abruptly different transport properties.[2]

VI. SUMMARY AND CONCLUSION

Using self-consistent LDA band theory, we are able to reproduce and partially understand the complicated and subtle reasons for titanium monoxide crystal formation. The first-row transition metals near the right-hand end have more contracted 3d orbitals and consequently their oxides have a high degree of ionicity. In these oxides, the Madelung energy is the major contribution responsible for crystal binding. For the relatively less compact Ti 3d orbital, the contribution from valence orbital overlap becomes important. The ordered vacancies allow the valence electrons to delocalize so as to lower the kinetic energy, thus stabilizing these struc-

tures. This decrease in kinetic energy, however, must be balanced against a loss of Madelung energy. The local-density approximation appears to correctly predict the balance between these competing factors. By examining a series of hypothetical $3d$ transition-metals compounds with the same structure, we find that this balance between Madelung- and kinetic-energy contributions is related to the size of the transition-metal d orbital. The mechanism we have described in which the vacancy-induced perturbation breaks the host rocksalt energy-level degeneracies into bonding and antibonding states should also be applicable to the technologically important refractory transition-metal carbides and nitrides with their thermodynamically stable defective structures.

ACKNOWLEDGMENTS

C. L. thanks N. Chetty for programming help in the resistivity calculation and many discussions. This work was supported by the Division of Materials Sciences, U.S. Department of Energy, under Contract No. DE-AC02-76CH00016, and by a grant of computer time at the National Energy Research Supercomputer Center.

[1] A. Neckel, Int. J. Quantum Chem. **23**, 1317 (1983).
[2] M. D. Banus, T. B. Reed, and A. J. Strauss, Phys. Rev. B **5**, 2775 (1972).
[3] D. Watanabe, J. R. Castles, A. Jostsons, and A. S. Malin, Acta Crystallogr. **23**, 307 (1967).
[4] V. Ern and A. C. Switendick, Phys. Rev. **137**, A1927 (1965).
[5] L. F. Mattheiss, Phys. Rev. B **5**, 290 (1972).
[6] A. Neckel, P. Rastl, R. Eibler, P. Weinberger, and K. Schwarz, J. Phys. C **12**, 3691 (1979).
[7] R. M. Wentzcovitch, Phys. Rev. B **44**, 2357 (1991).
[8] R. M. Wentzcovitch and J. L. Martins, Solid State Commun. **78**, 831 (1991).
[9] N. Troullier and J. L. Martins, Phys. Rev. B **43**, 1993 (1991).
[10] D. M. Ceperley and B. J. Alder, Phys. Rev. Lett. **45**, 566 (1980).
[11] J. P. Perdew and A. Zunger, Phys. Rev. B **23**, 5048 (1981).
[12] L. Kleinman and Bylander, Phys. Rev. Lett. **48**, 1425 (1982).
[13] A. Taylor and N. J. Doyle, in *The Chemistry of Extended Defects in Non-Metallic Solids*, edited by M. O'Keeffe (North-Holland, Amsterdam, 1970), p. 523.
[14] L. L. Van Zandt, J. M. Honig, and J. B. Goodenough, J. Appl. Phys. **39**, 594 (1968).
[15] C. E. Rice and W. R. Robinson, Acta Crystallogr. B **33**, 1342 (1976).
[16] J. F. Banfield, D. R. Veblen, and D. J. Smith, Am. Mineral. **76**, 343 (1991).
[17] The reference O_2 total energy (including spin-polarization energy), needed to calculate the heats of formation, was obtained by combining the results of non-spin-polarized O_2 total energies calculated using the same plane-wave pseudopotential method (with lattice constants up to $13.68a_B$ separating the O_2 molecules) with all-electron spin-polarized results for an isolated O_2 molecule [G. S. Painter and F. W. Averill, Phys. Rev. B **26**, 1781 (1982)].
[18] A. D. Pearson, J. Phys. Chem. Solids **5**, 316 (1958).
[19] D. W. Fischer, J. Appl. Phys. **41**, 3922 (1976).
[20] L. Pauling, *The Nature of the Chemical Bond*, 3rd ed. (Cornell University Press, Ithaca, 1960).
[21] J. Goodenough, Phys. Rev. B **5**, 2764 (1972).
[22] The overlap between the self-consistently calculated and model wave functions could be increased beyond this value by adjusting the relative amounts of each function. Since we are interested in the qualitative aspects, we have not attempted to do so.
[23] O. K. Andersen and S. Satpathy, in *Basic Properties of Binary Oxides*, edited by A. Dominguez Rodriguez, J. Castaing, and R. Marquez (Servicio de Publicationes de la Universidad de Sevilla, Sevilla, 1984).
[24] W. W. Schulz and R. M. Wentzcovitch, Phys. Rev. B **48**, 16 986 (1993).
[25] P. B. Allen, Comments Condens. Matter. Phys. **15**, 327 (1992).
[26] P. B. Allen, Phys. Rev. B **36**, 2920 (1987).
[27] B. A. Sanborn, P. B. Allen, and D. A. Papaconstantopoulos, Phys. Rev. B **40**, 6037 (1989).
[28] W. W. Schulz, L. Forro, C. Kendziora, R. Wentzcovitch, D. Mandrus, L. Mihaly, and P. B. Allen, Phys. Rev. B **46**, 14 001 (1992).
[29] Z. Fisk and G. W. Webb, Phys. Rev. Lett. **36**, 1084 (1976).
[30] J. Zak, *The Irreducible Representations of Space Groups* (Benjamin, New York, 1969).
[31] *Handbook of Chemistry and Physics*, 70th ed. (Chemical Rubber, Cleveland, 1989), p. D-90.